REPORT DOCUMENTATION PAGE

Public reporting burden for this collection of information is estimated to average 1 hour per response, including the time for reviewing instructions, searching existing data sources, gathering and maintaining the data needed, and completing and reviewing the collection of information. Send comments regarding this burden estimate or any other aspect of this collection of information, including suggestions for reducing this burden to Washington Headquarters Services, Directorate for Information Operations and Reports, 1215 Jefferson Davis Highway, Suite 1204, Arlington, VA 22202-4302, and to the Office of Management and Budget, Paperwork Reduction Project (0704-0188), Washington, DC 20503.

1. AGENCY USE ONLY (Leave Blank)	2. REPORT DATE 31 July 1998	3. REPORT TYPE AND DATES COVERED 6/98-5/99

4. TITLE AND SUBTITLE
Electric Field Effects in Ionization of Water Ice Layers on Platinum

5. FUNDING NUMBERS
N00014-97-1-0417

Richard Carlin

6. AUTHOR(S)

T. D. Pinkerton, D. L. Scovell, and E. M. Stuve

7. PERFORMING ORGANIZATION NAME(S) AND ADDRESS(ES)

University of Washington
Department of Chemical Engineering
Box 351750
Seattle, WA 98195-1750

8. PERFORMING ORGANIZATION REPORT NUMBER

Technical Report No. 9

9. SPONSORING / MONITORING AGENCY NAME(S) AND ADDRESS(ES)

Office of Naval Research
800 N. Quincy Street
Arlington, VA 22217

10. SPONSORING/MONITORING AGENCY REPORT NUMBER

11. SUPPLEMENTARY NOTES

Prepared for publication in Langmuir

19980817 080

12a. DISTRIBUTION / AVAILABILITY STATEMENT

This document has been approved for public release and sale; its distribution is unlimited.

12b. DISTRIBUTION CODE

13. ABSTRACT (Maximum 200 words)

Field ionization of water ice adsorbed onto a platinum field emitter tip of radius 350 Å was studied as a function of temperature over the range of 80–145 K and water layer thickness from 100 to 3000 Å. The water adlayer was grown under field-free conditions by exposure to water vapor in ultrahigh vacuum. Field ionization was probed by ramped field desorption (RFD) in which desorption of ionic species (hydrated protons) is measured while increasing the applied electric field linearly in time. The dependence of the field required for onset of ionization as a function temperature and thickness is presented and discussed. In the limit of thin water layers the onset field of ionization decreased from 0.6 to 0.3 V/Å with temperature increasing from 80 to 145 K. An activation barrier of 0.75 eV for ionization of water to produce hydrated protons and hydroxide ions was estimated from the temperature dependence of the onset field. The onset field increased with water layer thickness due to dielectric screening by water in qualitative agreement with the predictions of a previous model based on a spherical tip/water layer geometry and a variable permittivity of water. A breakpoint in the slope of onset field vs. thickness was interpreted as a transition in the ionization location from the water-vacuum interface to the tip-water interface. The relevance of these experiments in simulating electrode/electrolyte interfaces is discussed.

14. SUBJECT TERMS
Ionization, Water, Ice, Platinum, Electric field, Field desorption, Hydronium ion, Metal/Electrolyte Interface

15. NUMBER OF PAGES
25

16. PRICE CODE

17. SECURITY CLASSIFICATION OF REPORT	18. SECURITY CLASSIFICATION OF THIS PAGE	19. SECURITY CLASSIFICATION OF ABSTRACT	20. LIMITATION OF ABSTRACT
Unclassified	Unclassified	Unclassified	

NSN 7540-01-280-5500

Standard Form 298 (Rev. 2-89)
Prescribed by ANSI Std. 239-18
298-102

DTIC QUALITY INSPECTED 1

OFFICE OF NAVAL RESEARCH

"Electric Field Effects in Ionization of
Water Ice Layers on Platinum"

by

T. D. Pinkerton, D. L. Scovell, and E. M. Stuve

Prepared for Publication

in

Langmuir

University of Washington
Department of Chemical Engineering
Box 351750
Seattle, WA 98195-1750

July, 1998

ELECTRIC FIELD EFFECTS IN IONIZATION OF

WATER ICE LAYERS ON PLATINUM

T. D. Pinkerton, D. L. Scovell, and E. M. Stuve*

University of Washington

Department of Chemical Engineering

Box 351750

Seattle, WA 98195

*To whom correspondence should be addressed:
Phone: (206)543-0156
Fax: (206) 543-3778
E-mail: stuve@u.washington.edu

Abstract

Field ionization of water ice adsorbed onto a platinum field emitter tip of radius 350 Å was studied as a function of temperature over the range of 80–145 K and water layer thickness from 100 to 3000 Å. The water adlayer was grown under field-free conditions by exposure to water vapor in ultrahigh vacuum. Field ionization was probed by ramped field desorption (RFD) in which desorption of ionic species (hydrated protons) is measured while increasing the applied electric field linearly in time. The dependence of the field required for onset of ionization as a function temperature and thickness is presented and discussed. In the limit of thin water layers the onset field of ionization decreased from 0.6 to 0.3 V/Å with temperature increasing from 80 to 145. An activation barrier of 0.75 eV for ionization of water to produce hydrated protons and hydroxide ions was estimated from the temperature dependence of the onset field. The onset field increased with water layer thickness due to dielectric screening by water in qualitative agreement with the predictions of a previous model based on a spherical tip/water layer geometry and a variable permittivity of water. A breakpoint in the slope of onset field vs. thickness was interpreted as a transition in the ionization location from the water-vacuum interface to the tip-water interface. The relevance of these experiments in simulating electrode/electrolyte interfaces is discussed.

1. Introduction

Electrode/electrolyte interfaces typically support high surface electric fields on the order of 1-3 V/Å[1-3] — fields strong enough to make and break chemical bonds. While the surface electric field depends upon electrode potential and the nature of both electrode and electrolyte, the response of the electric field to these parameters and its subsequent influence in electrochemical processes remain unknown. To obtain an understanding of high surface electric fields in electrochemical phenomena, one seeks a method in which the electric field can be independently controlled. This is possible through adsorption studies involving water and electrolytic species on sharp field emitter tips in vacuum. Fields of 1 V/Å and larger (up to the limit of field evaporation of the tip) can be routinely obtained by application of potentials of 1–5 kV onto tips of radius 100–1000 Å. Because the tips themselves are nanometer-sized objects, studies of this nature are also relevant for understanding the role of water in process nanotechnology.

Despite the significance of field effects at water at electrode/electrolyte interfaces[4], there have been only a few studies of its behavior in high electric fields. Inghram and Gomer[5] first detected field ionized water clusters from a tungsten tip. Beckey[6,7] later showed that these clusters were hydrated protons $H^+ \cdot (H_2O)_m$ with m ranging from 1–10. He also reported the field assisted ionization of water to form hydrated protons; a field of only 0.15 V/Å was sufficient to ionize water in a thin layer (approximately 10 molecules thick) on a tungsten tip at liquid nitrogen temperature. Schmidt[8] reported critical ionization fields of 0.2 V/Å for water on a tungsten tip and 0.5 and 0.6 V/Å for tips of the noble metals iridium and platinum, respectively. Anway[9] examined field ionization in thick water layers, reported evidence for surface ionization as well as ionization within the water adlayer, and discussed the stability of the condensed water layer.

In more recent work Stintz and Panitz[10,11] introduced a new technique, isothermal ramped field desorption (RFD), to study irreversibly adsorbed water-ice adlayers below 150 K on tungsten, platinum, and iridium tips. The RFD technique is analogous to thermal desorption measurements,

one of the main techniques of surface science, and is the primary method used in this study. Unlike the earlier studies water is adsorbed onto the tip under field free conditions, so any preferential ordering in the ice layer represents that which would normally occur upon adsorption. As in the previous work the ramped field data of Stintz and Panitz show ionization of water ice to form hydrated protons with typically three waters per cluster. Other field ionization and field emission studies of water include measurements of ion energy deficits for ionization at rhodium tips[12], photon stimulated field ionization of water[13,14], real-time field ionization imaging of the hydrogen/oxygen reaction on a platinum tip[15,16], and field emission microscopy of water layers[17,18].

The electrochemical environment was simulated in this work by adsorption of thick water layers (100 to 3000 Å) onto a platinum field emitter tip. In such thick layers the dielectric property of water will screen the applied electric field such that the actual field will be a function of tip potential, thickness of the water layer, and position within the layer. The variation of electric field within the water layer was examined in a previous study[19] that showed that the electric field is concentrated at one or both interfaces of the system. For thin water layers the field is concentrated at the water-vacuum interface, whereas for thick water layers the field is concentrated, and even amplified, at the tip-water interface. From this modeling study we expect ionization to occur at the point of maximum field in the adlayer, which will be at one of the interfaces.

In this paper we report our first experimental results for field ionization of water. Water was adsorbed at temperatures of 80 to 145 K onto a platinum field emitter tip under field-free conditions in ultrahigh vacuum. Ionization was examined by RFD performed as a function of temperature and water layer thickness. We interpret the results in terms of the temperature and thickness dependence of the field of onset of ionization and compare the experimental results with those of the previous modeling study.

2. Equipment and Procedure

The experiments were performed in a stainless steel vacuum chamber, shown schematically in Fig. 1. The system was pumped by a turbo molecular pump and titanium getter pump to obtain a base pressure of 1×10^{-10} torr. A field emitter tip was used to generate electric fields as large as ~ 4 V/Å. Ions produced by the tip were projected onto a pair of chevron microchannel plates (MCP) and imaged onto a phosphor screen.

The tip was spot-welded to a 0.25 mm diameter heating loop mounted at the bottom of a cryogenically cooled downtube. Temperature was measured by a chromel/alumel thermocouple spot-welded to the tip shank, and the desired temperature was maintained by a PID temperature controller connected to a remotely programmable DC power supply for resistive heating. Temperatures as low as 100 K were obtained with liquid nitrogen, while temperatures below 50 K could be obtained with liquid helium cooling. The power supply and thermocouple reader were "floated" at the tip potential, while the PID controller was maintained at ground potential. Analog signals between the controller and power supply and thermocouple reader were transmitted along fiber optic cables through voltage-to-frequency and frequency-to-voltage converters at each end. This system provided effective high voltage isolation between the instruments of up to 20 kV. A high voltage feedthrough at the bottom of the downtube provided high voltage isolation for the heating loop/tip assembly.

The field emitter tip was electrochemically etched from 0.013 mm platinum wire at 1-3 V DC in a molten mixture of sodium chloride and sodium nitrate[20]. The tip radius was determined from the best imaging voltage in neon and calibration with the reported best-imaging field of 3.75 V/Å[20]. The relationship between applied potential V_t and applied field F_{app} is

$$F_{app} = V_t / \kappa r_t, \tag{1}$$

where κ is a geometrical factor (typically 5 for a conical tip[20]) and r_t the radius of the tip. The tip

radius in these experiments was 350 Å. The radius was also estimated by counting the number of lattice steps between the (001) and (113) planes. These two measurements agreed to within 20 %. The relative error in the electric fields reported in these experiments is less than 5 %. In this paper we use the term "applied electric field" to describe the field that would be present at a bare tip surface in vacuum for the tip potential applied in the experiment.

Before each experiment the tip was first cleaned by heating to ~ 500 K to desorb any water from the heating loop/tip assembly. Any contaminants not thermally desorbed were field desorbed while imaging the tip in a mixture of neon and hydrogen. By field desorbing a small amount of platinum, the surface was known to be atomically clean.

A uniform layer of water was deposited onto the tip maintained at the specified temperature under field-free conditions. The water used in these experiments was supplied by a Nano-pure water system with resistivity greater than 18 MΩ cm. The water was placed in a stainless steel reservoir and degassed in several freeze-thaw cycles with both liquid nitrogen and dry ice. Water vapor was introduced into the background of the vacuum chamber through a variable leak valve to ensure a uniform deposition. The tip was exposed to 5.0 x 10^{-7} torr of water for 2 to 60 minutes; after dosing pressures of less than 5 x 10^{-9} torr were typically reached within 5 to 10 minutes. The thickness of the water (ice) layer was estimated from the molecular flux determined by the time and pressure during dosing with a sticking coefficient of unity[21]. The ice density was allowed to vary linearly from 0.8 g/cm^3 at 80 K to 0.93 g/cm^3 at 130 K[21]. The estimated thickness of the ice layer was adjusted for any desorption that would have occurred while pumping down the chamber[21]. Water thicknesses of 100 to 3000 Å were obtained.

After the water was removed from the background a ramped field desorption[22] (RFD) spectrum was obtained. In the RFD experiments the potential applied to the tip was linearly increased with time at a rate of 10 V/s. When the applied field was large enough to create and desorb ions from the water, the ions were radially accelerated away from the tip. The signal from

4

the phosphor screen was capacitatively coupled to a pulse amplifier and monitored by two rate meters each with a time constant of 0.1 s. The first rate meter was always set to a sensitivity of 300 counts per second (CPS) full scale, while the second was adjusted so as to capture the entire peak. It was necessary to have the first rate meter set at a constant value in order to define an instrumental constant, which will be used later. A plotter equipped with a digital buffer recorded the analog signals from the two rate meters along with the tip potential. The rates were plotted against tip potential, which is proportional to the applied field (eq. 1), and transferred to a computer for storage and analysis. A CCD camera and VCR recorded field ionization images from the phosphor screen. These images provided spatial information to complement the RFD spectra.

3. Results

The effects of temperature and ice thickness were examined by two series of experiments. Figure 2 shows a series of spectra obtained at varying temperatures while holding the ice thickness constant. As the temperature increases the peaks shift to lower applied fields, with the exception of that at 130 K. At 80 K there is a small peak at 0.72 V/Å. With increasing temperature the small peak present at 80 K grows into a shoulder on the main peak, until at 130 K it becomes part of a three peaked structure.

RFD curves as a function of ice thickness at 110 K are shown in Fig. 3. The peak shifts to higher applied field with increasing coverage of water, and the leading edge of the desorption peak progressively broadens. For thick coverages of water, the peak ends with a spike as can be seen at a dimensionless thickness t/r_t of 4.2.

The onset field of ionization, defined experimentally as the field at which ionization reached 100 CPS in the RFD measurement, was measured as a function of ice thickness. The results of measurements at 110 K are shown in Fig. 4. The data show two linear regions with a break point at a dimensionless thickness of 1.7. This change in slope was present in all temperatures examined. Extrapolation of the line at low coverage to zero thickness gives an estimate of the actual field needed for ionization. (Extrapolation is necessary to correct for the field in the ice layer being different from the applied field, see below.) The extrapolated onset fields for several different temperatures are shown in Fig. 5. The onset of ionization varies linearly with temperature between 80 and 145 K.

A CCD camera and VCR recorded the images on the phosphor screen during the field ramp. For thin layers ionization was always uniform and randomly distributed about the tip surface. The ionization for thick layers (above the break point of the onset field vs. thickness curve) was localized to several points that were approximately evenly spaced about the tip.

4. Discussion

Temperature Dependence

The temperature dependence of the onset field of ionization provides information about the energetics of the ionization event. For thermally excited ionization the rate of ionization may be written as

$$r_{ion} = n_w \nu \exp[-Q(F)/kT], \tag{2}$$

where n_w is the areal density of water molecules (1×10^{15} cm^{-2}), ν the pre-exponential factor (3×10^{15} s^{-1})[21], $Q(F)$ the field dependent activation energy, k Boltzmann's constant, and T temperature. In the charge exchange model[23] ionic desorption occurs when the field shifts the ionic desorption curve to a sufficiently low energy. This is illustrated qualitatively in Fig. 6. The field dependent activation barrier for ionic desorption is given by

$$Q(F) = V(x_c) + H_a - (\Delta P)F - \tfrac{1}{2}(\Delta \alpha)F^2 - \tfrac{1}{2}\Delta E_{res}, \tag{3}$$

where $V(x)$ is the potential energy curve as a function of distance from the surface, x_c the distance where ionization occurs, H_a the field-free activation barrier, P the dipole moment, α the polarizability and ΔE_{res} the energy splitting at the avoided crossing between neutral and ionic potential energy curves. The Δ term in the dipole moment and polarizability term signifies that the value is the difference between the final and initial states. (Fig. 6 shows a dipolar interaction $P_i F$ only for the initial state.) In general, the last term on the right hand side of eqn. (3) is negligible, and at the fields used in this work the polarizability term is also small in comparison to the dipolar interaction term. Thus, the activation barrier simplifies to

$$Q \approx V(x_c) + H_a - (\Delta P)F. \tag{4}$$

7

Since the applied field alters the ionic potential curve (shown as the thick dashed line), the potential energy at the curve crossing is also a function of field. If we assume (for simplicity) that the neutral and ionic potential energy curves are straight in the region of the crossing (shown by the thin lines crossing at x_c), then we can approximate the potential energy as

$$V(x_c) = V_0 + V_1 F + \dots , \tag{5}$$

where higher order terms would be used for non-linear curve crossings. Equation (5) indicates the variation of x_c with applied field. The zero order term is easily seen to be zero since the field free barrier is already represented by H_a. Also, note that V_1 must be negative for a field activated process.

As a constant detection rate was used to determine the onset of ionization, these data represent an instrumental constant I_c which can be estimated from eqn. (2)

$$I_c = -\ln\left(\frac{r_{ion,o}}{n_w V}\right) = \frac{Q(F_o)}{kT} , \tag{6}$$

where $r_{ion,o}$ is the specified ionization rate and F_o the onset field. Combination of eqns. (4) - (6) and elimination of Q thus gives

$$F_o = \frac{1}{V_1 - \Delta P}\left(H_a - I_c k\, T\right). \tag{7}$$

This expression predicts a linear relationship between the onset field of ionization and the temperature, as observed in Fig. 5. A similar linear relationship, in excellent agreement with these results, was reported by Stintz and Panitz[11]. Extrapolation of the data to zero field provides an

estimate of the field free activation barrier, given knowledge of the instrumental constant. To estimate the instrumental constant, we approximate the rate of ionization as the rate of detection N_{ion} per area of the tip imaged by the detector. The latter we estimate as a hemisphere based on the tip radius

$$r_{ion,o} = \frac{N_{ion}}{2\pi r_t^2}.$$
(8)

From the specified detection rate (100 CPS) and tip radius (350 Å) the instrumental constant is $I_c = 40$. With an extrapolated temperature of 220 K the field-free activation barrier for ionization of condensed water is thus 0.75 eV.

The activation barrier for ionization applies to a process that produces desorbed hydrated protons. A general reaction for this may be written as

$$(n + m + 1)\ H_2O_a\ \longrightarrow\ OH^- \cdot (H_2O)_{n,a} + H^+ \cdot (H_2O)_{m,g}$$
(9)
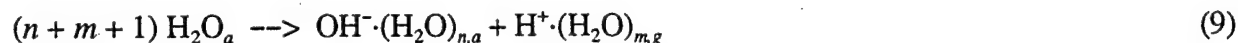
in which ionization leaves a fully hydrated hydroxide ion in the ice layer and ejects a hydrated proton. As the RFD measurements were not mass resolved the distribution of hydrated proton clusters is not known. Experiments under similar conditions[11] indicate a value of 3 for m. The field free activation barrier of 0.75 eV for ion emission exceeds that for desorption of neutral water of 0.5 eV[24]. Still, the barrier is quite low and indicates the relative ease of ionization in water adlayers. As a point of reference, the barrier value is approximately equal to the energy of three hydrogen bonds. This result indicates that water layers deposited at cryogenic temperatures can be expected to be nonionic, as 0.75 eV barriers are difficult to cross at temperatures of 170 K and below, but the barrier is not so large as to prevent autoprotolysis of water to form H_3O^+ and OH^- at room temperature.

The charge exchange analysis represented by eqn. (7) and Fig. 6 leaves many other questions unanswered, however. For example, the exact natures of the neutral and ionic potential energy curves in Fig. 6 are largely unknown due to the complex arrangement of solvating water molecules. The onset field data show that thermal excitation is significant in the ionization process, but whether the barrier is crossed by thermal excitation, or by thermally excited tunneling, in which thermal excitation is required to reach a slightly higher lying final state by proton tunneling, is unclear. Furthermore, the slope of the onset field vs. temperature data cannot be easily deconvoluted for the relative importance of the curve crossing (V_1) vs. dipolar interaction (ΔP) effects. The slope of -0.0043 V Å^{-1} K^{-1} is equivalent to a dipole moment of 3.8 Debye, a value approximately twice that of water of 1.8 Debye. There are a number of possible explanations for the magnitude of the temperature dependence, yet none can be singled out as most likely. For example, if one were to attribute the result to dipolar interactions only, the structures of the initial and final states, and their corresponding dipole moments, are not at all clear.

Thickness Dependence

As the thickness of the ice layer increases, the applied field needed to initiate ionization also increases. This is easily explained by dielectric screening of the water layer, thicker water layers being more effective at screening the field at the water-vacuum interface. Comparison of the experimental results with our previous modeling study of the field distribution in water adlayers allows for a more quantitative description of the thickness dependence.

The water/tip system was modeled in spherical geometry; the tip was assumed to be a perfect conductor and a variable permittivity was used for the water layer[19]. The potential distribution was found by numerical solutions to Poisson's equation for the water layer and Laplace's equation for the vacuum. The relative permittivity of the water was allowed to vary between low and high field limits of 80 and 2, respectively, with the transition occurring between 0.01 and 1 V/Å[25]. The

potentials in both the water layer and vacuum were calculated as a function of tip potential and water thickness. This model assumes that there are no ions present in the water layer. It was found that the fields were always concentrated at the tip-water and water-vacuum interfaces.

Figure 7 shows a plot of lines of constant electric field for varying thickness of water and applied electric field. The lower curve represents the locus of points where the field at the water-vacuum interface F_v is equal to 0.5 V/Å, the value obtained by the extrapolation in Fig. 4, while the upper curve represents the same for the tip-water interface F_t. This model predicts that for thin layers of water, the predominant field will be at the water-vacuum interface and ionization will be initiated there. If the water layer is thick enough, the variable permittivity concentrates the field at the tip surface, and the predominant field will be at the tip-water interface. Thick layers are predicated to have ionization initiate at the tip surface. The experimental data from Fig. 3 are also shown in Fig. 7. The change in slope occurs at about the same dimensionless thickness for the model and experimental data, although the slope of the data is substantially different from the predictions of the model. The model predicts a decrease in the applied field required to produce ions for coverages above the break point, in contrast to our results. The change in slope at the break point can be explained by the creation of ions at the tip surface that are bound up and solvated by hydrogen bonding to other water molecules. Positive ions created at the tip surface would be repelled from the positively charged surface and would migrate towards the water-vacuum interface. This excess positive charge in the water layer would increase the electric field at the vacuum interface, thereby reducing the applied field needed for ionization at that interface.

Even though the model qualitatively fits the data, there are substantial differences between the two. One possibility is that the model underpredicts the field for a given thickness. The permittivity used in the model was calculated for 300 K, while these experiments were performed at cryogenic temperatures. Increasing the model permittivity would increase the model field such that a lower applied field would be necessary to achieve the specified model field in the water layer.

11

Even a constant permittivity of infinity (perfect conductor) cannot make the model fit the data, however. Another possibility is that our model overpredicts the ice thickness. The model assumes a uniform deposition and does not allow for surface diffusion or possible restructuring due to the electric field during the RFD measurement. A third possibility is that the two-dimensional nature of the field emitter tip is not well suited to a one-dimensional, spherical model. Finally, the model does not allow for the presence of ions in the water layer. Observation of localized ionization in the RFD images of thick water layers suggests the presence of ions. In such cases the detected ions would result from field enhancement at the water-vacuum interface by the embedded ions, as discussed above. Verification of this effect, as well as answers to the questions raised above, are the subject of continuing experimental and theoretical studies in our laboratory.

5. Conclusions

Field ionization of water layers adsorbed under field-free conditions on a platinum tip occurs for fields of 0.6 to 0.3 V/Å over a temperature range of 80 to 145 K. From these results and the charge exchange model for ionic desorption the field-free activation barrier for ionization of water to produce hydrated protons and hydroxide ions is estimated to be 0.75 eV. Field ionization occurred for all thicknesses of water layers studied. Thicker water layers require a higher applied field for ionization because of dielectric screening by the water layer itself. Qualitative agreement was obtained between the experimentally measured onset field of ionization and the predictions of a model based on a spherical geometry. A breakpoint in the onset field vs. thickness curve is tentatively assigned to a change in ionization location from the water-vacuum to the tip-vacuum interface, according to the model prediction; this occurred at a dimensionless water thickness of t/r_t = 1.7 at 110 K. Discrepancies between the data and the model predictions were interpreted in terms of limitations and assumptions of the model.

References

1)Price, D.; Halley, J. W. *J. Electroanal. Chem.* **1983**, *159*, 347-353.

2)Kreuzer, J. *Surface Sci.* **1991**, *246*, 336-347.

3)Schmickler, W. *Surface Sci.* **1995**, *335*, 416-21.

4)Cocke, D. L.; Block, J. H. *Surface Sci.* **1978**, *70*, 363-391.

5)Inghram, M. G.; Gomer, R. *Z. Naturforschg.* **1955**, *10a*, 863.

6)Beckey, H. D. *Z. Naturforschg.* **1959**, *14a*, 712-721.

7)Beckey, H. D. *Z. Naturforschg.* **1960**, *15a*, 822-827.

8)Schmidt, W. A. *Z. Naturforschg.* **1964**, *19a*, 318-327.

9)Anway, A. R. *J. Chem. Phys.* **1969**, *50*, 2012-2021.

10)Stintz, A.; Panitz, J. A.; *J. Vac. Sci. Tech. A* **1991**, 9, 1365-1367.

11)Stintz, A.; Panitz, J. A. *Surface Sci.* **1993**, *296*, 75-86.

12)Tsong, T. T. *J. Vac. Sci. Tech. B* **1985**, *3*, 1425-1430.

13)Dirks, J.; Drachsel, W.; Block, J. H. *J. Vac. Sci. Tech. B* **1992**, *10*, 231-234.

14)Sotola, J.; Drachsel, W.; Block, J. H. *Surface Sci.* **1992**, *266*, 70-75.

15)Ernst, N.; Bozdech, G.; Gorodetskii, V.; Kreuzer, H. J.; Wang, R. L. C.; Block, J. H. *Surface Sci.* **1994**, *318*, L1211-1218.

16)Gorodetskii, V.; Ernst, N.; Drachsel, W.; Block, J. H. *Appl. Surf. Sci.* **1995**, *87*, 151-158.

17)Bryl, R.; Blaszczyszyn, R.; Galewska, E. *Vacuum* **1997**, *48*, 329-332.

18)Ciszewski, A.; Blaszczyszyn, R. *Prog Surface Sci.* **1995**, *48*, 99-108..

19)Scovell, D. L.; Pinkerton, T. D.; Finlayson, B. A.; Stuve, E. M. *Submitted to Chem. Phys. Letters* **1998**.

20)Tsong, T. T. *Atom-probe field ion microscopy - Field ion emission and surface and interfaces at atomic resolution*; Cambridge University Press: Cambridge, 1990.

21)Brown, D. E.; George, S. M.; Huang, C.; Wong, E. K. L.; Rider, K. B.; Smith, R. S.; Kay, B.

D. *J. Phys. Chem.* **1996**, *100*, 4988-4995.

22)Stintz, A.; Panitz, J. A.; *J. App. Phys.* **1992**, *72*, 741-745.

23)Gomer, R. *Field emission and field ionization*; Harvard University Press: Cambridge, 1961.

24)Thiel, P. A.; Madey, T. E. *Surface Sci. Reports* **1987**, *7*, 211-385.

25)Huinink, H. P.; deKeizer, A.; Leermakers, F. A. M.; Lyklema, J. *J. Phys. Chem.* **1996**, *100*, 9948-9954.

Figure Captions

Fig. 1 - Schematic of field ionization apparatus.

Fig. 2 - Ramped field desorption curves (total ion intensity) of ice layers of thickness $t/r_t = 0.7$ as a function of temperature.

Fig. 3 - Ramped field desorption curves (total ion intensity) of ice layers adsorbed at 110 K as a function of thickness.

Fig. 4 - Applied field at onset of ionization as a function of ice thickness for 110 K.

Fig. 5 - Applied field at onset of ionization as a function of temperature in the limit of zero thickness of ice.

Fig. 6 - Illustration of the major terms used in the charge exchange model. The illustrated reaction is hydrogen transfer from one water molecule to another water molecule interacting by a hydrogen bond. The solid and dashed heavy lines represent hypothetical potential energy curves for neutral and ionic species, respectively. The applied electric field F is represented by the dotted line and lowers the energy of the ionic potential curve. The assumption of linear potential energy curves at the curve crossing is shown by the two intersecting thin solid lines. An example of a dipolar interaction for the initial state P_iF is shown by the dashed potential curve.

Fig. 7 - Model predictions of applied field necessary to obtain fields at the vacuum-water interface F_v and the tip-water interface F_t 0.5 V/Å. Experimentally measured onset fields of ionization at 110 K are shown for comparison.
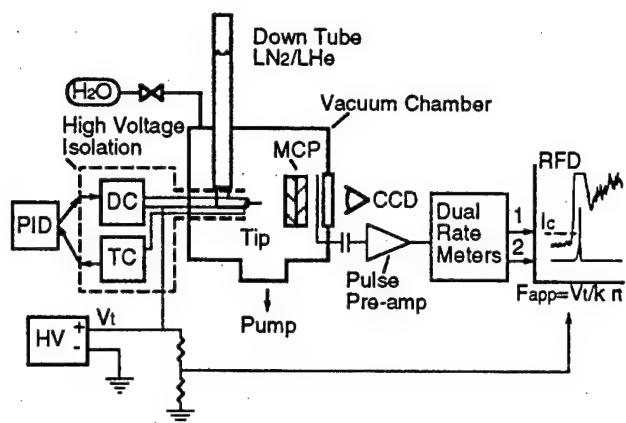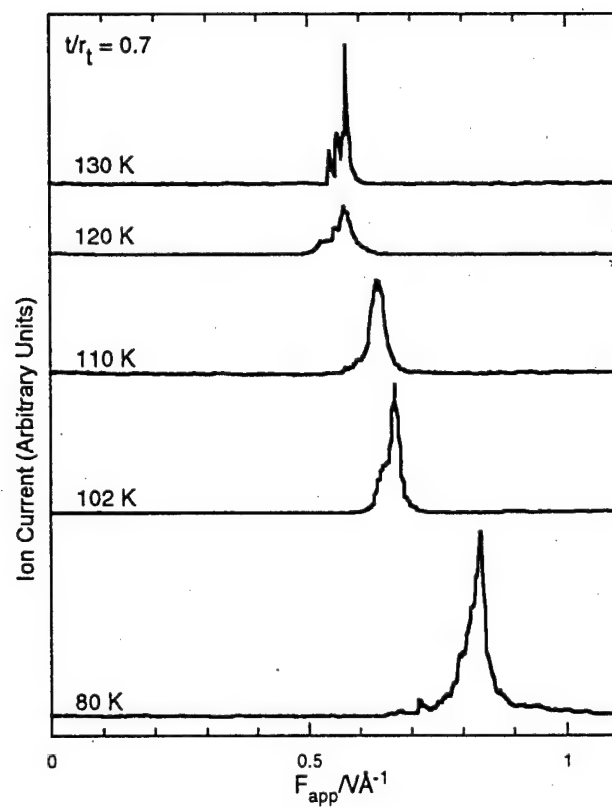
Fig. 1

Pinkerton, Scovell, Stuve
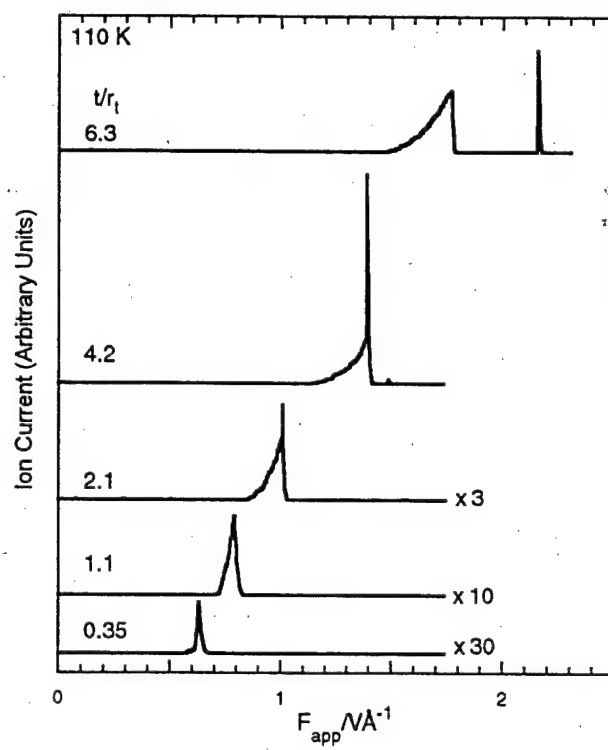
Fig. 2

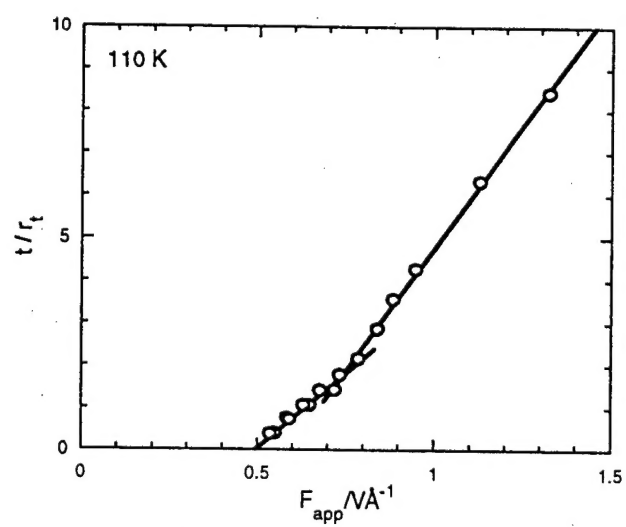Pinkerton, Scovell, Stuve

Fig. 3
Pinkerton, Scovell, Stuve

Fig. 4
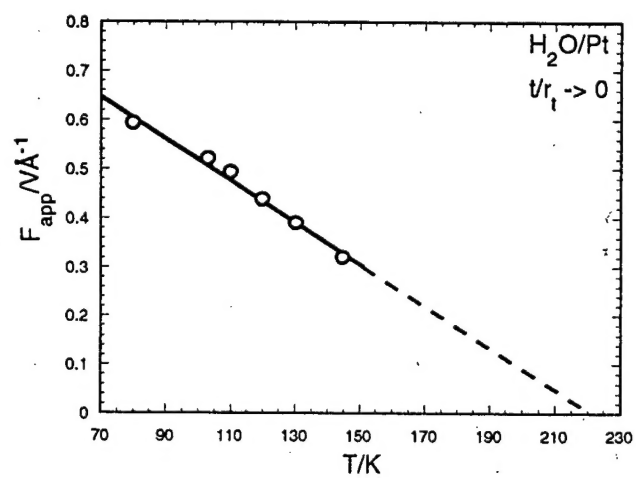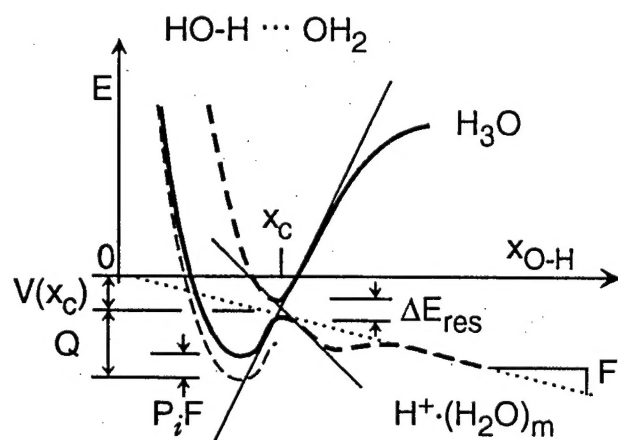
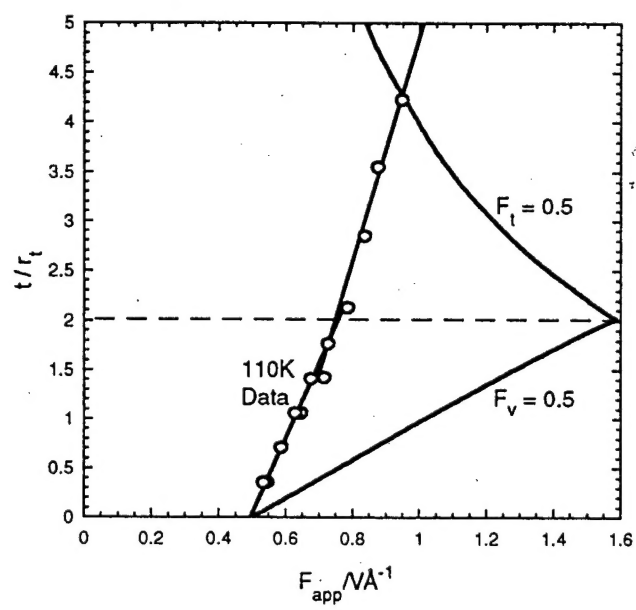Pinkerton, Scovell, Stuve

Fig. 5

Pinkerton, Scovell, Stuve

Fig. 6

Pinkerton, Scovell, Stuve

Fig. 7
Pinkerton, Scovell, Stuve